

Diamond photonics platform enabled by femtosecond laser writing

Belén Sotillo¹, Vibhav Bharadwaj¹, J. P. Hadden², Masaaki Sakakura⁴, Andrea Chiappini³, Toney Teddy Fernandez¹, Stefano Longhi¹, Ottavia Jedrkiewicz⁶, Yasuhiko Shimotsuma⁵, Luigino Criante⁷, Roberto Osellame¹, Gianluca Galzerano¹, Maurizio Ferrari³, Kiyotaka Miura⁵, Roberta Ramponi¹, Paul E. Barclay², Shane Michael Eaton^{1,*}

¹*Istituto di Fotonica e Nanotecnologie (IFN) – CNR and Dipartimento di Fisica, Politecnico di Milano*

²*Institute for Quantum Science and Technology, University of Calgary, Calgary, Canada*

³*CNR-IFN, CSMFO Lab. and FBK-CMM, Trento, Italy*

⁴*Office of Society-Academia Collaboration for Innovation, Kyoto University, Kyoto, Japan.*

⁵*Department of Material Chemistry, Graduate School of Engineering, Kyoto University, Kyoto, Japan*

⁶*Istituto di Fotonica e Nanotecnologie, CNR and CNISM Udr Como, Como, Italy*

⁷*Center for Nano Science and Technology, Istituto Italiano di Tecnologia, Milano, Italy*

*Corresponding author : shane.eaton@gmail.com

Usually admired for its aesthetics, diamond has other important qualities that make it useful for technological applications: it is the hardest known naturally occurring substance, it offers record high thermal conductivity and is transparent to ultraviolet light. Researchers have recently discovered that diamond is also an ideal substrate for spintronics and quantum information, which could lead to a practical quantum computer or ultrasensitive magnetic field detectors.[1,2] Analogous to semiconductors and conventional electronics, the key to making diamond functional are the properties of an impurity: the nitrogen-vacancy (NV) center, which are naturally incorporated during chemical vapour deposition (CVD) synthesis. At the negatively charged NV center, two adjacent sites in diamond's tetrahedral lattice of carbon atoms are altered: one with nitrogen while the other is vacant. The electrons of the NV center, largely localized at the vacancy site, combine to form a spin triplet, which can be polarized with 532-nm laser light, even at room temperature. One of the spin states fluoresces much more brightly than the others so that fluorescence intensity can be used for spin-state readout. The

NV center's states are isolated from environmental perturbations allowing spin coherence times (~1 ms) comparable to trapped ions.[3] These properties make diamond NV centers very attractive as a scalable platform for efficient sensing based on electron spins [4] and for quantum information systems.[5]

Applications such as magnetic field sensing and coherent storage of light in NVs could greatly benefit from the enhanced interaction of light provided by optical waveguides containing NV ensembles.[6] The fabrication of optical waveguides in diamond to connect NV centers is also compelling for quantum processing based on long-range entanglement.[7] However, the difficulty of creating single crystal diamond structures with a refractive index profile compatible for vertical waveguiding, such as a thin diamond film, is a significant hurdle for the fabrication of integrated optics in diamond. To harness the true potential of diamond NVs, a photonics fabrication toolkit similar to the one that has revolutionized silica planar lightwave circuits [8] and silicon photonics [9] is desirable.

Diamond waveguiding has been realized using a high refractive index material supported by a diamond substrate,[10,11] but this approach is limited by weak evanescent coupling to NVs near the sample surface. Single-crystal thin diamond films for waveguiding can be generated using the ion implantation assisted lift-off method,[12,13], however the thin films suffer from residual stress that make them detrimental for photonics applications. Another approach uses heterogeneous diamond growth followed by oxygen plasma etching to create membranes enabling both photonic crystals [14] and ring resonators [15,16], however it remains a significant challenge to remove tens of microns of diamond while maintaining smooth features needed for photonics applications. Further, post-fabrication annealing is often required to stabilize low-density NV emitters, leading to degradation in device performance [17].

Using a novel angled plasma etching process, suspended triangular nanobeam waveguides were recently demonstrated by the Lončar group [18,19] with waveguide propagation losses less than 10 dB/cm at visible wavelengths. The disadvantage of the angled-etching method is that for each device, a custom-made Faraday cage is needed to provide the correct angle deflection of the oxygen plasma. In a related technique, Khanaliloo *et al.* have demonstrated waveguides using diamond isotropic etching without a Faraday cage but as with the other techniques described, the fabricated optical circuits are limited to 2D geometries [20].

We propose a disruptive technology based on femtosecond laser writing to realize a 3D photonics toolkit for bulk diamond. We apply femtosecond laser writing [21] to directly inscribe 3D photonic circuits inside diamond in a single process step. Femtosecond laser written waveguides benefit from facile coupling with standard optical fibers for more efficient device implementation compared to other waveguide fabrication methods. Optical waveguides in bulk diamond could be used to optically link or address NVs, to enable efficient excitation and collection, and make integrated optic quantum information systems and spin-based sensing a reality.

Femtosecond laser writing relies on the nonlinear absorption of focused ultrashort pulses, which leads to a localized modification in the bulk of transparent materials. In glasses, this permanent modification is a positive refractive index change, and by translating the sample with respect to the incident laser using computer-controlled motion stages, low-loss waveguides with arbitrary 3D architectures can be formed.[21-29] However in crystals, a decrease in refractive index occurs since the lattice is damaged by the laser interaction,[30,31] which is a roadblock for optical waveguide formation. One further difficulty of writing in diamond is that previous works have shown that ultrashort laser pulses induce the strongly absorbing graphite phase.[32,33]

In this paper, we laser-write closely spaced parallel lines in diamond, to produce a stress-induced refractive index increase between them. We found that the 1000-fold higher repetition rate interaction compared to previous work [33,34] enables waveguiding of visible wavelengths. By tailoring the modification line spacing and geometry, we demonstrate single mode waveguiding from 532 nm to 800 nm, suitable for excitation and collection at nitrogen vacancy centers for magnetometry and quantum information. We also find that the optical emission and spin properties of NV ensembles in the waveguide are unchanged compared to those in the unpatterned regions.

Femtosecond laser writing experiments were performed with an oil immersion microscope objective with a numerical aperture (NA) of 1.25. Employing such a high NA allows for a smaller focal volume, to minimize the writing power and avoid self-focusing (critical power 2 MW at 515 nm), which leads to vertically elongated waveguide cross sections and non-reproducible results.[34] At 500 kHz repetition rate, we found that an average power of 50 mW and a scan speed of 0.5 mm/s along $\langle 110 \rangle$ crystallographic directions produced uniform and reproducible modifications in the bulk of diamond. As shown in the optical microscope image in **Fig. 1(a)**, the cross section of the laser-written track was approximately 5 μm transversely and 22 μm vertically. The significant vertical elongation of the line is attributed to the large spherical aberration caused by the mismatch between the index matching oil ($n = 1.5$) and diamond ($n = 2.4$). This asymmetry in the modification could be corrected using an adaptive optics approach.[34]

To better understand the structure of the femtosecond laser-written lines, μRaman spectroscopy was performed. As a reference, the pristine diamond has a characteristic Raman peak centered at 1332 cm^{-1} with a typical full width at half maximum (FWHM) of around 2.3 cm^{-1} . [35] For the above mentioned laser processing conditions, μRaman characterization (Fig.

1(b)) revealed that within the modification, there is a reduction of the intensity of the peak at 1332 cm^{-1} to 15% of the original intensity along with an increase of its width by about 2 cm^{-1} , evidencing increased disorder in the diamond lattice. Moreover, at least two new bands appear: the G-peak at 1575 cm^{-1} and the D-peak at 1360 cm^{-1} , showing a transformation of the sp^3 bonding of diamond into sp^2 bonding. In our case, the widths of D and G peaks (greater than 100 cm^{-1}) and the intensity ratio between them ($I(D)/I(G)$ less and close to 1) indicate that these sp^2 clusters are mainly in an amorphous carbon phase rather than graphite.[36] This is in contrast to previous work with 1-kHz repetition rate Ti:Sapphire femtosecond lasers,[32] which demonstrated the formation of micrographitic lines in diamond, which are not suitable for photonic devices. In fact, when we reduce the repetition rate from 500 kHz to 5 kHz, we observe a sharper G-peak with a slight displacement to higher wavenumber (Fig. 1(c)), which implies a greater concentration of nanocrystalline graphite clusters.[37] We also found that the second order peaks at 2700 cm^{-1} (2 D peak) and 2900 cm^{-1} (D + G peak) appear for 5 and 25 kHz, but not for 500 kHz, evidencing increased graphitization at these lower repetition rates.

Motivated by the μ Raman results at 500 kHz repetition rate, we attempted to form waveguides in diamond using the type II method to produce an increase in refractive index in the stressed region between two closely inscribed modification lines.[38] **Figure 2(a)** shows the transverse optical microscope image of the pair of laser-inscribed lines written $50\text{ }\mu\text{m}$ below the surface using the same laser processing conditions as the single line in Fig. 1(a). For $13\text{-}\mu\text{m}$ line separation, we produced for the first time to our knowledge, a buried optical waveguide in diamond. While the waveguide showed single mode behavior when scanning the input launch fiber transversely, when scanned vertically, modes could be excited at three different depths: the lowest loss mode was centered between the modification lines, as shown in Fig. 2(a). A mode could also be excited a few microns above and below this position (not shown in Fig.

2(a)). The mode field diameter (MFD) of the central and lowest loss mode is $10\ \mu\text{m} \times 11\ \mu\text{m}$ at 635 nm wavelength with an insertion loss of 14 dB using butt-coupled single mode fibers (including a coupling loss of 2.8 dB/facet, Fresnel reflection loss of 0.3 dB/facet and propagation loss of 16 dB/cm). We attribute the propagation loss mainly to scattering loss due to the overlap of the optical mode with the modification tracks. The propagation loss would be much higher should graphite be present in the laser-written lines. By evaluating the attenuation of the optical mode [39] we estimate a waveguide damping loss of greater than 10^4 dB/cm for type II modification tracks containing graphite.

At 532 nm, the wavelength for incoherent excitation of NV centers in diamond, the MFD was $9\ \mu\text{m} \times 9\ \mu\text{m}$ and similar losses were found compared to 635 nm wavelength. By using an end-fire free-space coupling setup with an adjustable polarizer at the input, we found that the type II waveguide from Fig. 2(a) supported only the TM mode. Similar polarization-dependent behavior has been reported in type II waveguides in other crystals such as lithium niobate,[38] KDP,[31] and Ti:Sapphire [40] and can be attributed to the elliptical shape of the modification, which results in a different stress-induced refractive index distribution for TE and TM polarizations.[38]

We further confirmed that 500-kHz offers a better regime for type II modification of diamond by lowering the repetition rate of the laser to 5 kHz. In this case, for powers of 1 – 5 mW (200 nJ to 1 μJ pulse energy) and track separations of 10 to 18 μm , we could not observe any waveguiding at visible wavelengths. Waveguiding may be impeded by increased graphitization at lower repetition rates (Fig. 1(c)) resulting in higher absorption of the launched visible light, supported by absorption measurements on samples with tracks written over the entire $5\ \text{mm} \times 5\ \text{mm}$ area (20 μm spacing between lines at 50 μm depth). As shown in Fig. 1(d), for visible wavelengths, the absorption is slightly higher for lower repetition rate processing.

We also found that the optical bandgap was reduced for 5 kHz processing, which is expected when graphitic inclusions are present.[41]

To achieve single mode guiding, we wrote a second vertically offset type II modification (Fig. 2(b)). This four-line modification supported a single mode at 635 nm wavelength with a MFD of $9 \mu\text{m} \times 10 \mu\text{m}$, an insertion loss of 19 dB and a coupling loss of 2.4 dB/facet. Similar to the case of the two-line type II waveguide, the four-line structure supported only the TM mode. Although each of the four lines shown in Fig. 2(b) was written with the same laser processing conditions, the vertical elongation of the lines increases dramatically with depth due to increased spherical aberration.[34] As described above, the motivation for using such a high NA is to reduce the fluence needed during fabrication to avoid nonlinear focusing. However, employing such a high NA will cause stronger spherical aberration from the refractive index mismatch between the diamond and index matching oil/microscope objective, leading to an axial distortion of the focused laser beam. To enable more symmetric modifications in bulk diamond, a spatial light modulator could be employed to impose a phase profile that is equal and opposite to the aberration introduced by the refractive index mismatch. This would allow more flexible and precise 3D patterning of the barrier zones of the type II waveguide, enabling a more symmetric four-line structure or even an annular type modification for confining light.

μ Raman measurements in diamond are sensitive to the presence of stress in the material. A shift of the diamond peak to higher (lower) wavenumber is associated with a compressive (tensile) stress. In **Fig. 3(a)** we present a map showing the peak shift near two laser written tracks. It can be seen that inside the guiding region the stress is mainly compressive, with a shift of about $+1.5 \text{ cm}^{-1}$ compared to pristine diamond. Tensile stress is mainly located at the top and bottom tips of the tracks. This result agrees with the model developed for type II guides in lithium niobate,[38] where the change in volume inside the laser-formed tracks creates a stress

around them that produces an increase in the refractive index in the region between the laser modifications. A similar shift in the diamond peak is observed at the center of the four-line type II structure (Fig. 3(b)), where the compressive stress covers a smaller region vertically.

A closer inspection of the Raman peak reveals that it is not only shifted, but also split into two components, as can be seen in Fig. 3(c), where spectra were fit to Lorentzian curves. This split is associated with the presence of biaxial or uniaxial stress between the two modification lines, rather than hydrostatic stress.[42] The stress field creates an anisotropy in the change in the refractive index, inducing the different behavior of the TE and TM modes reported above. Similar splitting of the Raman peak was observed for the four-line structure.

The type II modification is beneficial for quantum information and magnetometry applications relying on NV centers, since the waveguide mode propagates in the undamaged region between the laser-inscribed lines. Photoluminescence (PL) characterization using a confocal microscope revealed a reduction in the intensity of the NV's zero phonon line (ZPL) transition within the modification lines (**Fig. 4(a)**). However, in the region between the modification lines where the optical mode propagates, the PL spectrum was the same as that of pristine diamond. By launching 532-nm light into the waveguide and collecting the light using a spectrometer, we found a similar PL spectrum as that obtained by confocal microscopy (Fig. 4(b)). As the waveguide only supported the TM mode, the difference in the PL recorded from the TM and the TE configuration (shadowed in Fig. 4(b)) is the actual contribution of the guiding region to the PL, compared to the bulk material excited around the guide (Fig. 4(b) inset). These PL measurements provide strong evidence that the concentration of NV centers within the waveguide was not reduced by the laser-writing process. Within the modification lines, a bright signal was observed between 730 nm and 800 nm, which is attributed to the GR1 color center (740 nm) associated with neutral vacancies [43] created by laser writing. It is

possible that other vacancy complexes and interstitial defects are also induced causing spectral features similar to the radiation B Band of diamond which has undergone ion implantation and annealing.[44]

The reduction in graphitization with MHz-repetition rates compared to kHz rates may be due to the higher temperatures driven by the higher pulse delivery rate. Jerng *et al.* observed that above growth temperatures of 1100°C, amorphous carbon was produced instead of nanocrystalline graphite films.[45] In agreement with characterization by μ Raman spectroscopy, absorption and waveguide transmission, we have found that the electrical conductivity of lines written with the femtosecond laser is increased at lower repetition rates [46]. Future characterization including electro-chemical etching of the laser-written lines will seek to provide more insight into the modifications induced within the MHz repetition rate regime exploring other exposure parameters such as beam shaping with the SLM, pulse duration and wavelength. It is possible that the femtosecond laser-induced defects in the near-infrared (Fig. 4(a)) may assist in triggering the graphitization when processing the 800-nm laser wavelength of Ti:Sapphire lasers or the 1- μ m fundamental wavelength of Yb-based femtosecond lasers.

Optically detected magnetic resonance (ODMR) characterization within the buried diamond waveguides showed hyperfine structure, indicating that the electronic ground state of the NV centers was not adversely affected by femtosecond laser inscription. Further, the lifetime of the excited state transition (11.0 ± 1.5 ns) was the same for NV centers within the waveguide and pristine diamond. We are currently performing spin coherence measurements to confirm that the spin coherence of NV centers within the optical waveguide is preserved.

Working at room temperature, magnetometry devices based on NV ensembles [47] would benefit from waveguides for efficient collection and routing of the fluorescence signal. Even

more compelling is a diamond waveguide device with integrated Bragg reflectors at green and infrared wavelengths, to enable an integrated cavity enhanced magnetometer.[48] Bragg gratings waveguides have been demonstrated in glass by periodically modulating the intensity of the femtosecond laser pulse train during waveguide writing,[49,50] and a similar approach will be applied to diamond. Diamond waveguides with Bragg reflection functionality would enable a significant enhancement of the magnetic-field sensitivity since the cavities increase the absorption path length by a factor proportional to their finesse.[51]

Diamond has shown itself as an important material for quantum photonics, being a host to defect centers with atom-like properties having long-lived spin quantum states and well-defined optical transitions. The 3D photonics toolkit that we have developed to manipulate and route light efficiently while preserving the astonishing properties of NV centers may help diamond reach its full potential for quantum technologies.

References

- [1] L. Childress, R. Walsworth, M. Lukin, *Phys. Today* **2014**, *67*, 38.
- [2] L. Childress, J. M. Taylor, A. S. Sørensen, M. Lukin, *Phys. Rev. A* **2005**, *72*, 052330.
- [3] G. Balasubramanian, P. Neumann, D. Twitchen, M. Markham, R. Kolesov, N. Mizuochi, J. Isoya, J. Achard, J. Beck, J. Tissler, V. Jacques, P. R. Hemmer, F. Jelezko, J. Wrachtrup, *Nat. Mater.* **2009**, *8*, 383.
- [4] R. Schirhagl, K. Chang, M. Loretz, C. L. Degen, *Annu. Rev. Phys. Chem.* **2013**, *65*, 83.
- [5] B. Hensen, H. Bernien, A. E. Dréau, A. Reiserer, N. Kalb, M. S. Blok, J. Ruitenber, R. F. L. Vermeulen, R. N. Schouten, C. Abellán, W. Amaya, *Nature* **2015**, *526*, 682.
- [6] I. Aharonovich, A. D. Greentree, S. Praver, *Nat. Photonics* **2011**, *5*, 397.
- [7] H. J. Kimble, *Nature* **2008**, *453*, 1023.
- [8] C. R. Doerr, K. Okamoto, *J. Lightwave Technol.* **2006**, *24*, 4763.

- [9] R. Soref, *IEEE J. Sel. Top. Quant.* **2006**, *12*, 1678.
- [10] K. M. Fu, C. Santori, P.E. Barclay, I. Aharonovich, S. Praver, N. Meyer, A. M. Holm, R. G. Beausoleil, *Appl. Phys. Lett.* **2008**, *93*, 234107.
- [11] P. E. Barclay, K. M. C. Fu, C. Santori, A. Faraon, R. G. Beausoleil, *Phys. Rev. X* **2011**, *1*, 011007.
- [12] P. Olivero, S. Rubanov, P. Reichart, B. C. Gibson, S. T. Huntington, J. Rabeau, A. D. Greentree, J. Salzman, D. Moore, D. N. Jamieson, S. Praver, *Adv. Mater.* **2015**, *17*, 2427.
- [13] J. C. Lee, I. Aharonovich, A. P. Magyar, F. Rol, E. L. Hu, *Opt. Express* **2012**, *20*, 8891.
- [14] B. J. M. Hausmann, B. J. Shields, Q. Quan, Y. Chu, N. P. De Leon, R. Evans, M. J. Burek, A. S. Zibrov, M. Markham, D. J. Twitchen, H. Park, *Nano Lett.* **2013**, *13*, 5791.
- [15] A. Faraon, P. E. Barclay, C. Santori, K. M. C. Fu, R. G. Beausoleil, *Nat. Photonics* **2011**, *5*, 301.
- [16] B. J. M. Hausmann, I. Bulu, V. Venkataraman, P. Deotare, M. Lončar, *Nat. Photonics* **2014**, *8*, 369.
- [17] M. J. Burek, Private Communication
- [18] M. J. Burek, Y. Chu, M. S. Liddy, P. Patel, J. Rochman, S. Meesala, W. Hong, Q. Quan, M. D. Lukin, M. Lončar, *Nat. Comm.* **2014**, *5*, 5718.
- [19] M. J. Burek, N. P. De Leon, B. J. Shields, B. J. M. Hausmann, Y. Chu, Q. Quan, A. S. Zibrov, H. Park, M. D. Lukin, M. Lončar, *Nano Lett.* **2012**, *12*, 6084.
- [20] B. Khanaliloo, H. Jayakumar, A. C. Hryciw, D. P. Lake, H. Kaviani, P. E. Barclay, *Phys. Rev. X* **2015**, *5*, 041051
- [21] K. M. Davis, K. Miura, N. Sugimoto, K. Hirao, *Opt. Lett.* **1996**, *21*, 1729.
- [22] S. M. Eaton, H. Zhang, P. R. Herman, F. Yoshino, L. Shah, J. Bovatsek, A. Arai, *Opt. Express* **2005**, *13*, 4708.
- [23] R. R. Gattass, E. Mazur, *Nat. Photonics* **2008**, *2*, 219.

- [24] T. Meany, L. A. Ngah, M. J. Collins, A. S. Clark, R. J. Williams, B. J. Eggleton, M. J. Steel, M. J. Withford, O. Alibart, S. Tanzilli, *Laser Photonics Rev.* **2014**, *8*, L42.
- [25] S. Nolte, M. Will, J. Burghoff, A. Tünnermann, *Appl. Phys. A* **2003**, *77*, 109.
- [26] A. Crespi, Y. Gu, B. Ngamsom, H. J. Hoekstra, C. Dongre, M. Pollnau, R. Ramponi, H. H. van den Vlekkert, P. Watts, G. Cerullo, R. Osellame, *Lab Chip* **2010**, *10*, 1167.
- [27] A. Szameit, Y. V. Kartashov, F. Dreisow, T. Pertsch, S. Nolte, A. Tünnermann, L. Torner, *Phys. Rev. Lett.* **2007**, *98*, 173903.
- [28] R. R. Thomson, T. A. Birks, S. G. Leon-Saval, A. K. Kar, J. Bland-Hawthorn, *Opt. Express* **2011**, *19*, 5698.
- [29] A. Ródenas, G. Martin, B. Arezki, N. Psaila, G. Jose, A. Jha, L. Labadie, P. Kern, A. Kar, R. Thomson, *Opt. Lett.* **2012**, *37*, 392-394.
- [30] J. Burghoff, C. Grebing, S. Nolte, A. Tünnermann, *Appl. Phys. Lett.* **2006**, *89*, 081108.
- [31] L. Huang, P. Salter, M. Karpiński, B. Smith, F. Payne, M. Booth, *Appl. Phys. A* **2015**, *118*, 831.
- [32] B. Sun, P. S. Salter, M. J. Booth, *Appl. Phys. Lett.* **2014**, *105*, 231105.
- [33] S. M. Pimenov, I. I. Vlasov, A. A. Khomich, B. Neuenschwander, M. Muralt, V. Romano, *Appl. Phys. A* **2011**, *105*, 673.
- [34] R. D. Simmonds, P. S. Salter, A. Jesacher, M. J. Booth, *Opt. Express* **2011**, *19*, 24122.
- [35] J. W. Ager III, D. K. Veirs, G. M. Rosenblatt, *Phys. Rev. B* **1991**, *43*, 6491.
- [36] J. Schwan, S. Ulrich, V. Batori, H. Ehrhardt, S. R. P. Silva, *J. Appl. Phys.* **1996**, *80*, 440.
- [37] A. C. Ferrari, J. Robertson, *Phys. Rev. B* **2000**, *61*, 14095.
- [38] J. Burghoff, S. Nolte, A. Tünnermann, *Appl. Phys. A* **2007**, *89*, 127.
- [39] A. B. Djurišić, E. H. Li, *J. Appl. Phys.* **1999**, *85*, 7404.
- [40] J. Bai, G. Cheng, X. Long, Y. Wang, W. Zhao, G. Chen, R. Stoian, R. Hui, *Opt. Express* **2012**, *20*, 15035.

- [41] K. B. K. Teo, S. E. Rodil, J. T. H. Tsai, A. C. Ferrari, J. Robertson, W. I. Milne, *J. Appl. Phys.* **2001**, *89*, 3706.
- [42] Y. Kaenel, J. Stiegler, J. Michler, E. Blank, *J. Appl. Phys.* **1996**, *81*, 1726.
- [43] I. Kiflawi, A. T. Collins, K. Iakoubovskii, D. Fisher, *J. Phys.-Condens. Mat.* **2007**, *19*, 046216.
- [44] A. M. Zaitsev in *Optical Properties of Diamond*, Springer Berlin Heidelberg, Germany, **2001**, pp. 152-154
- [45] S. K. Jerng, D. S. Yu, Y. S. Kim, Junga Ryou, Suklyun Hong, C. Kim, S. Yoon, D. K. Efetov, P. Kim, S. H. Chun, *J. Phys. Chem. C* **2011** *115*, 4491.
- [46] M. Girolami, L. Criante, S. Lo Turco, A. Mezzetti, A. Notargiacomo, M. Pea, A. Bellucci, P. Calvani, F. di Fonzo, V. Valentini, D. M. Trucchi “Graphite distributed electrodes for diamond-based photon-enhanced thermionic emission solar cells” (Submitted)
- [47] H. Clevenson, M. E. Trusheim, C. Teale, T. Schröder, D. Braje, D. Englund, *Nat. Phys.* **2015**, *11*, 393.
- [48] J. M. Taylor, P. Cappellaro, L. Childress, L. Jiang, D. Budker, P. R. Hemmer, A. Yacoby, R. Walsworth, M. D. Lukin, *Nat. Phys.* **2008**, *4*, 810.
- [49] G. D. Marshall, M. Ams, M. J. Withford, *Opt. Lett.* **2006**, *31*, 2690.
- [50] H. Zhang, S. M. Eaton, P. R. Herman, *Opt. Lett.* **2007**, *32*, 2559.
- [51] O. Gazzano, C. Becher, *arXiv preprint* **2016**, *arXiv:1603.04529*.

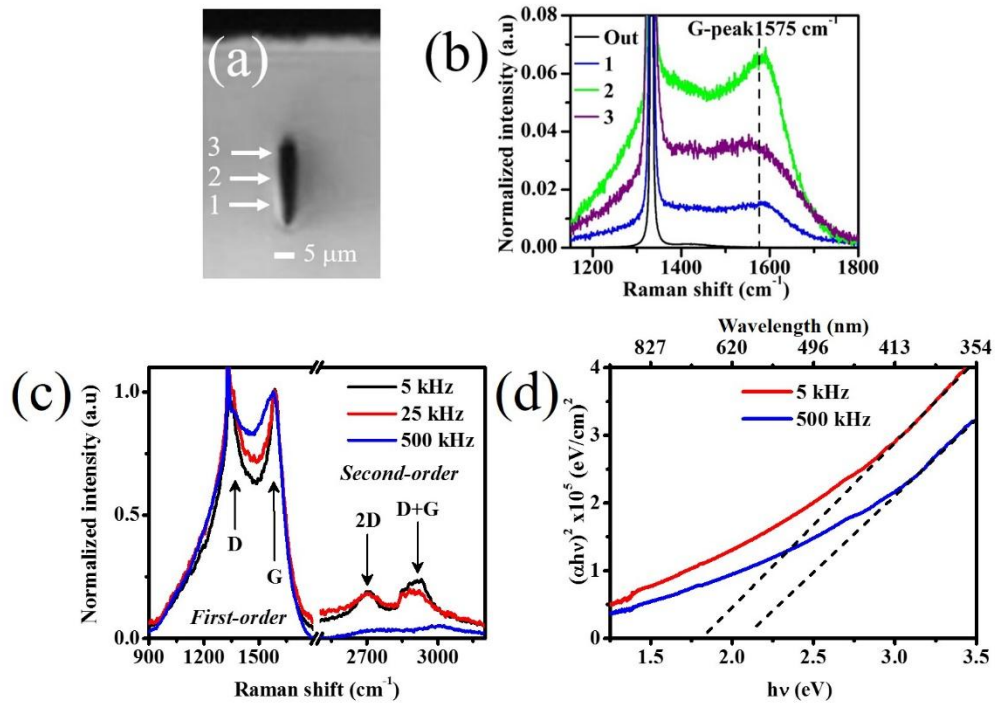


Figure 1. (a) Transverse optical microscope image of single laser-induced track written with 500-kHz repetition rate, 50-mW average power and 0.5-mm/s scan speed. (b) μ Raman spectra (532-nm excitation wavelength) at four different vertical positions inside the modification. ‘Out’ refers to a spectrum taken outside the track. The spectra have been normalized to the diamond peak to show the change in the relative intensity of the G-peak inside the structure. (c) μ Raman spectra (normalized to the G-peak) in the center of modification tracks at repetition rates of 5 kHz, 25 kHz and 500 kHz, with pulse energy held constant (800 nJ) to produce a similar size modification at each repetition rate. (d) Tauc plot for diamond with tracks written over the entire sample at 50- μ m depth and 20- μ m line separation for 5-kHz and 500-kHz repetition rates. It is considered that the absorption in the visible region is only due to the modification tracks, with the rest of the sample being transparent.

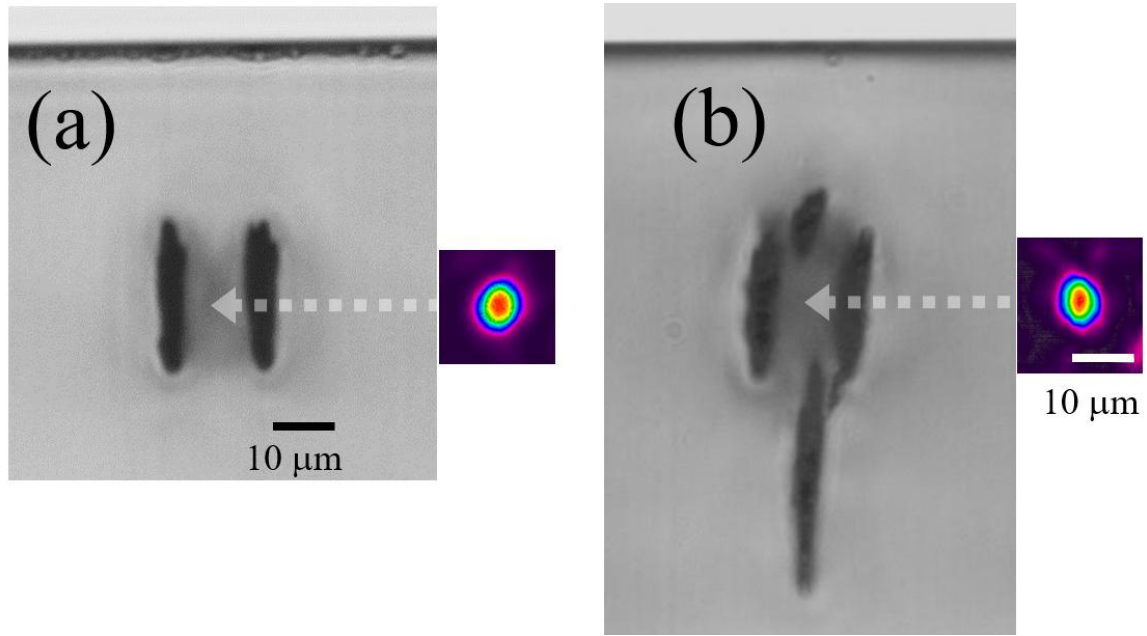


Figure 2. Transverse microscope view of type II waveguide in diamond along with near field mode profile ($\lambda = 635$ nm). An arrow indicates the position of the mode. (a) Pair of lines, horizontally separated by $13 \mu\text{m}$. Modes could be coupled into three different vertical positions with the lowest loss mode shown (MFD $10 \mu\text{m} \times 11 \mu\text{m}$). (b) Pair of lines, horizontally separated by $13 \mu\text{m}$ along with second pair of lines for vertical confinement. Only a single mode could be coupled to the four-line modification (MFD $9 \mu\text{m} \times 10 \mu\text{m}$). All tracks were written with 50 mW , 0.5 mm/s at 500 kHz with deeper tracks more elongated due to increased spherical aberration.

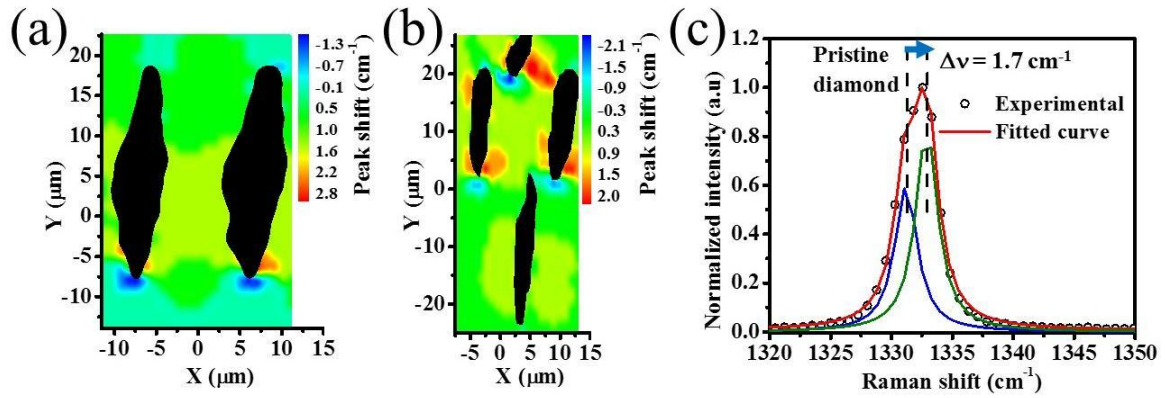


Figure 3. Spatial map frequency shift of diamond Raman peak with respect to bulk for (a) two-line and (b) four-line modification, with the same parameters as those in Figure 2. The modification tracks are shown as black. (c) Diamond Raman peak measured between two modification lines horizontally separated by 13- μm , along with the fit to two Lorentzian curves, showing the shift and split of the peak respect to the pristine material.

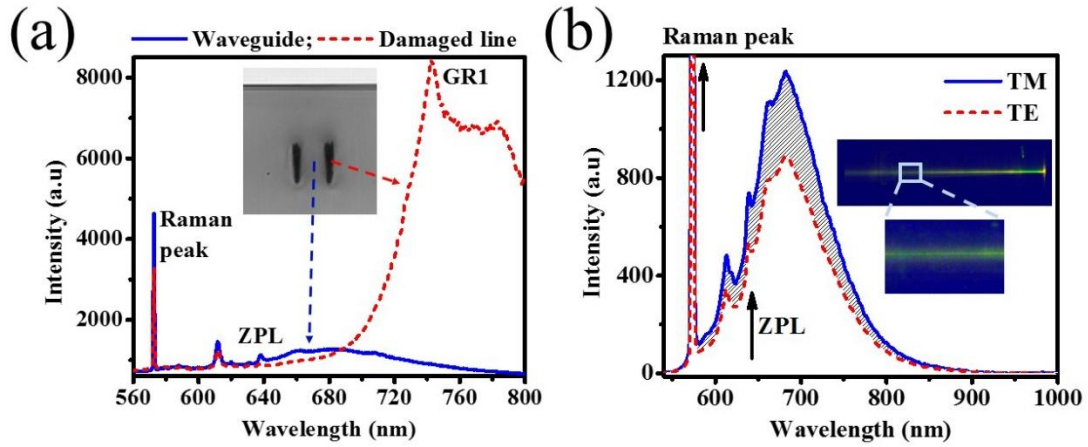


Figure 4. (a) Photoluminescence spectra within the laser-written lines (red spectrum) and between the modification lines in the waveguiding region (blue spectrum) acquired by confocal microscopy (excitation wavelength 532 nm). A cross sectional microscope image of the type II waveguide from Fig. 1(a) is shown in the inset. Both spectra show the first order Raman shift line at 573 nm, the ZPL of the NV center at 637 nm along with its associated broad phonon sideband from 600 nm – 800 nm. The spectrum in pristine diamond is the same as that in the waveguide region. (b) Photoluminescence detected with spectrometer at output of the waveguide when light was coupled in using free space optics (TM and TE configurations are presented). The inset shows an overhead microscope image of the fluorescence streak when the 532-nm light was coupled to the waveguide.

Experimental

The femtosecond second laser used for waveguide writing in diamond was a regeneratively amplified Yb:KGW system (Pharos, Light Conversion) with 230-fs pulse duration, 515-nm wavelength (frequency doubled), focused with a 1.25-NA oil immersion lens (RMS100X-O 100× Olympus Plan Achromat Oil Immersion Objective, 100× oil immersion, Olympus). The polarization of the incident laser was perpendicular to the scan direction. The repetition rate of the laser was variable from 1 MHz to single pulse. Computer-controlled, 3-axis motion stages

(ABL-1000, Aerotech) interfaced by CAD-based software (ScaBase, Altechna) with an integrated acousto-optic modulator (AOM) were used to translate the sample relative to the laser to form the desired photonic structures.

Polished 5 mm × 5 mm × 0.5 mm synthetic single-crystal diamond samples (type II, optical grade with nitrogen impurities 100 ppb) were acquired from MB Optics. Laser-inscribed structures were characterized for their morphology using white-light optical microscopy in transmission mode with 10× and 40× magnification objectives (Eclipse ME600, Nikon).

For waveguide transmission measurements, high resolution 3-axis manual positioners (Nanomax MAX313D, Thorlabs) were used. The four-axis central waveguide manipulator (MicroBlock MBT401D, Thorlabs) enabled transverse displacement between sets of diamond waveguides. Light sources at 808 nm (S1FC808, Thorlabs), 635 nm (TLS001-635, Thorlabs) and 532 nm (4301-010, Uniphase) were coupled to the waveguides using the appropriate Thorlabs single-mode fibers for each of the visible wavelengths (460HP for 532 nm, SM600 for 635 nm, 780HP for 808 nm). To test the polarization dependence of the waveguide transmission, free-space coupling was used with 10× (5721-H-B, Newport) and 60× (5721-H-B, Newport) lenses at the input and output, respectively. At the output, light was coupled to an optical power meter (818-SL, Newport) to measure the power transmitted through the waveguide. To measure the near-field waveguide mode profile, a 60× asphere (5721-H-B, Newport) was used to image the light to a beam profiler (SP620U, Spiricon).

Micro-Raman spectra were recorded using a Labram Aramis Jobin Yvon Horiba microRaman system with a DPSS laser source of 532 nm and equipped with a confocal microscope and an air-cooled CCD. A 50× (100×) objective was used to focus the laser on the sample as well as to collect the Raman signal, with a spatial resolution of about 1 micron. A wavenumber accuracy of about 1 cm⁻¹ can be achieved with a 1800 line/mm grating.

To observe the characteristic fluorescence from the negatively charged NV center at 637 nm (and the phonon sidebands), 532-nm light from a 1-W frequency-doubled Nd:YVO₄ laser (Verdi, Coherent) was coupled with and collected with the free space optics described above and detected with a spectrometer (Ocean Optics model HR2000). A notch filter in the green was used to attenuate the pump wavelength.

For confocal photoluminescence measurements, nitrogen-vacancy defects were excited with a DPPS 532-nm laser (CL532-500-L, CrystaLaser) focused on to the sample with a 0.55 NA objective (100X Plan Apo SL Infinity Corrected Objective, Mitutoyo). Photoluminescence was collected through the same objective, filtered from the excitation light using a dichroic beamsplitter (ZT 532 RDC, Chroma) and long-pass filters (ET 555 LP Chroma, FELH 0650 Thorlabs) and focused into a single mode fibre which provided the confocal aperture. Photon counting of the filtered light was performed using an avalanche photodiode (SPQR-14, Perkin-Elmer). Optically detected magnetic resonance measurements were performed by monitoring the fluorescence rate while scanning the frequency of a microwave field driven through a 20 μ m copper wire on the surface of the sample generated using a commercial microwave source (Agilent ESG E4433B) amplified by a high power broad band amplifier (Minicircuits ZHL-16W-43+)

Acknowledgements

This work has been supported by the FP7 DiamondFab CONCERT Japan project, DIAMANTE MIUR-SIR grant, and FemtoDiamante Cariplo ERC reinforcement grant. We thank Michael Burek and Patrick Salter for helpful scientific discussions. We gratefully thank Ursula Klabbers of MB Optics (Velp, Netherlands) for assistance in post-polishing of the diamond samples.